Available online at www.sciencedirect.com

ScienceDirect

Procedia CIRP 129 (2024) 139–144

www.elsevier.com/locate/procedia

18th CIRP Conference on Computer Aided Tolerancing (CAT2024)

Evaluation of Reconstruction Methods in X-ray Computed Tomography Geometric Measurement

Kaojie Yue*, Huan Shao, Stefano Petrò, Giovanni Moroni

Department of Mechanical Engineering, Politecnico di Milano, Via La Masa 1, Milano 20156, Italy

* Corresponding author. Tel.: +39 3475440654. *E-mail address:* kaojie.yue@polimi.it

Abstract

In X-ray Computed Tomography (XCT) geometric measurement, the reconstruction process is a main step that significantly influences acquisition strategies and measurement results. Analytical algorithms, primarily Feldkamp-Davis-Kress (FDK), and algebraic algorithms are commonly used for reconstruction, with FDK being the dominant choice for dimensional measurements. Although algebraic algorithms offer advantages like denoising and handling limited projections, their evaluation concerning measurement accuracy remains insufficient. To assess the performance with respect to measurement accuracy and sensitivity to acquisition parameters, we performed typical reconstruction algorithms on the measurements of diameter, cylindricity, and flatness, including FDK and ordered subsets simultaneously algebraic reconstruction technique (OS-SART). Moreover, the algorithm comprised in a commercial software was used and evaluated. Variables in acquisition included part orientation and exposure time. The analysis comparing XCT measurements with those from Coordinate Measuring Machine showed different performances of the two reconstruction algorithms and the potential of algebraic algorithms in XCT geometric measurement.

Keywords: X-ray computed tomography; Geometric measurement; Reconstruction algorithm

1. Introduction

X-ray Computed Tomography (XCT), as a technique for nondestructive testing, has been widely used in industrial applications such as defect detection [1], [2]. In recent years, XCT was also used for dimensional inspection to verify the geometric quality of the parts. This is attributed to its ability to measure internal dimensions, and its measurement time independent of part's complexity. With the development and application of additive manufacturing which allows complex and internal features, XCT geometric measurement has become a great interest for researchers [3], [4]. Basically, XCT geometric measurement includes four steps: data acquisition, reconstruction, surface determination, and dimensional measurements [3]. In this process, reconstruction involves recreating the part's geometry from the projection images acquired during data acquisition. Two primary types of reconstruction algorithms exist, with the widely utilized Feldkamp-Davis-Kress (FDK) standing out as a typical analytical algorithm, serving as the main reconstruction algorithm in geometric measurement applications [4]. The other category is algebraic algorithms, which have gained popularity in medical XCT due to advantages in dose reduction, noise estimation, and high speed [5], [6], [7], [8]. In recent years, algebraic reconstruction algorithms have been introduced in geometric measurements to enhance acquisition efficiency [9], [10], [11]. However, since the principle and process of two algorithms are quite different, they may lead to different measurement accuracy, even when using the same dataset. Moreover, the impact of acquisition parameters on measurement results may differ from reconstruction algorithms. Therefore, it is necessary to evaluate the reconstruction algorithms in the XCT geometric measurement, including measurement accuracy and the sensitivity to acquisition parameters.

10.1016/j.procir.2024.10.025

The assessment of the FDK algorithm was mentioned in several studies, and Villarraga-Gómez et al. [4] summarized the results of CT-Audit, CIA-CT and InteraqCT comparisons, showing the range of the quoted uncertainties. Additionally, investigations into the impact of certain acquisition parameters on measurement accuracy have been conducted. Villarraga-Gómez et al. [12] studied the influence of number of projections (*Np*) on the measurement of length, diameter, hole distance, flatness, and cylindricity. It was found that reducing *Np* causes the decrease of reconstruction quality, resulting in minor effects on size dimensions but noticeable errors in form dimensions. In another study by the same authors, it was demonstrated that part orientation, defined as the angle between the rotation axis and the part central axis, influences measurements of diameter, length, and roundness. Minimum deviation was obtained when the orientation is within 10° to 35° [13]. Furthermore, decreasing geometric magnification generally leads to larger deviations in the diameter and roundness of holes [14]. The work of Rossides et al. [15] highlighted that a shorter exposure time induces biases in cylinder diameters. Collectively, these studies gave guidance to optimize the acquisition strategy and achieve high measurement accuracy.

The performance of algebraic reconstruction algorithms was also investigated. Jones et al. [9] tested several algebraic reconstruction algorithms applied in medical domain, specifically evaluating their performance in measuring location of edges and wall thickness. Results showed the potential of these algorithms in improving acquisition efficiency. In diameter measurements, Rossides et al. [15] observed apparently biases and larger variances when using algebraic reconstruction algorithms (CGLS and FISTA-TV), compared with that using FDK algorithm. Sun et al. [10] measured the size of inner/outer cylinders and cuboids on simulated dataset, using less than 2% data of a full scan. It was found that two algebraic algorithms (OS-SART and OS-ASD-POCS) yielded values close to the nominal values. Currently, most studies on algebraic reconstruction algorithms in XCT geometric measurement focus on using a smaller number of projections to obtain accurate dimensional measurement results [10], [11], [15]. It is unclear whether the impact of acquisition parameters on measurements using algebraic reconstruction algorithms aligns with that observed in the FDK reconstruction algorithm.

In this study, we assessed the results of XCT geometric measurements using three reconstruction algorithms: FDK algorithm, ordered subset simultaneously algebraic reconstruction technique (OS-SART), and the reconstruction algorithm of a commercial software (Phoenix Datos|x). Focusing on the measurement of diameter, cylindricity, and flatness, the main effects of reconstruction algorithms and two acquisition parameters (part orientation and exposure time) on measurement results were analyzed. Furthermore, we explored the interactions among reconstruction algorithms and acquisition parameters.

2. Methodology

2.1. Data collection

The part used in this work (Fig. 1) is a five steps multi-cylinder. The bottom part serves only as fixturing. Before XCT scans, the part was calibrated on a Zeiss Prismo VAST HTG coordinate measuring machine located in a controlled environment at 20±0.5 ℃. The measurands and their nominal values are listed in Table 1. The data acquisition process was performed on a Phoenix V|tome|x M300 XCT system as shown in Fig. 2, comprising a 300 kV microfocus X-ray tube and a Dynamic 41|100 detector with 2016×2016 pixels of 200 µm physical dimension. During the acquisition, to save time and scan data amount, the active area of the detector was reduced to 1500×2016 pixels.

Detailed acquisition parameters are shown in Table 2, where the number of projections was determined referring to Nyquist-Shannon sampling theorem [10], [16], and each image was obtained averaging 5 images. Two additional factors were considered, each varying on two levels: exposure time and part orientation. Part orientation was defined as the angle from rotation axis to the part center axis. Experiments were replicated twice, with random re-positioning the part and recalibrating the sensor after each scan. In total 8 experiments were performed in a randomized order, with the room temperature at 20±3 ℃. Calibration of the XCT system was performed before the experiment, and image calibrations were conducted before each scan.

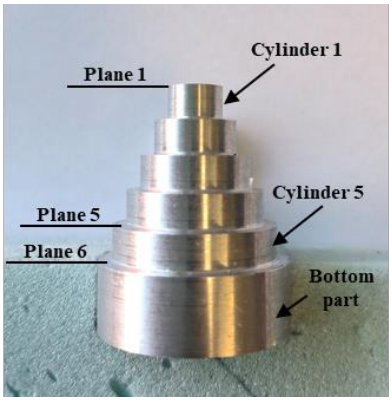

Fig. 1. Part geometry

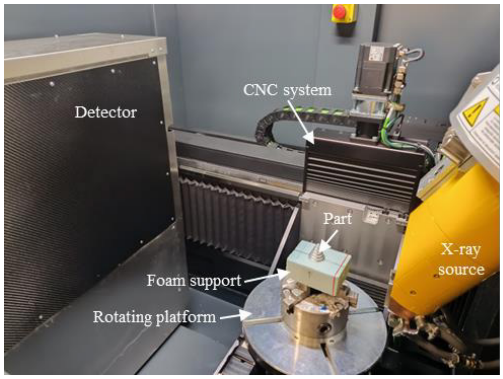

Fig. 2. X-ray computed tomography system.

Table 1. Nominal dimensions of the part.

Measurands	Name	Nominal value /mm
Diameter of cylinder 1	D1	8
Diameter of cylinder 2	D2	12
Diameter of cylinder 3	D3	16
Diameter of cylinder 4	D4	20
Diameter of cylinder 5	D5	24
Cylindricity of cylinder 1	Cy1	N/A
Cylindricity of cylinder 2	Cy2	N/A
Cylindricity of cylinder 3	Cy3	N/A
Cylindricity of cylinder 4	Cy4	N/A
Cylindricity of cylinder 5	Cy5	N/A
Flatness of plane 1	F1	N/A
Flatness of plane 2	F2	N/A
Flatness of plane 3	F3	N/A
Flatness of plane 4	F4	N/A
Flatness of plane 5	F5	N/A
Flatness of plane 6	F6	N/A

Table 2. Parameters and setups in data acquisition.

Constant parameters	Setups
X-ray tube voltage /kV	250
X-ray tube current /μA	100
Voxel size /μm	32.294
Scan mode	Start/stop
Average	5
Number of projections	2356
Filter material	Sn
Filter thickness /mm	1.0
Binning	1×1
Variables	Values
Part orientation /°	0, 45
Exposure time/ms	50, 100

2.2. Reconstruction algorithms

After data acquisition, three reconstruction algorithms were used for reconstruction. The first algorithm was FDK which represents the analytical reconstruction method, containing three steps: (1) weighting the projection data; (2) filtering the weighted projection data; (3) performing back-projection process [17]. The second algorithm was OS-SART [18], a typical algebraic reconstruction algorithm, with 20 images (default setup) in each subset. The last one was proprietary algorithm of the XCT system (Phoenix Datos|x, referred to as Phoenix for convenience). The first two algorithms were from TIGRE [19], a graphic process unit (GPU) based reconstruction toolkit and were executed in Matlab 2022b. Parameters related to the algorithm were set as default values. The reconstruction processes were performed on a computer with the following configuration: CPU: Intel(R) Xeon(R) W-2225, GPU: NVIDIA Quadro RTX 5000, Memory: 256 GB.

2.3. Dimension extraction and data analysis

To obtain the dimensions in voxel models from the reconstruction, surface determination and dimensional measurement were performed in Volume Graphic Studio Max (VGS). To ensure accuracy, the advanced (classic) surface determination with the searching distance of 4 voxels and iterative determination was utilized [20]. The features were recognized and fitted automatically in the software, with guidance from a few manually selected surface points. Dimensions were then obtained using VGS.

After XCT measurement, the error between XCT measurement results and calibrated sizes/deviations was used as the response variable for ANOVA. With 5 cylinders, 6 planes, 3 reconstruction algorithms, 2 acquisition parameters (with 2 levels), and 1 duplicate considered, the experiment yielded 120 diameter results, 120 cylindricity results, and 144 flatness results. Main effects of reconstruction algorithm and acquisition parameters were analyzed, and the interactions between them were also examined.

3. Results

3.1. Voxel model

Voxel models were obtained with an average computation time equal to 810 s for FDK and 18385 s for OS-SART. The voxel models after the surface determination are shown in Fig. 3 (from the experiment with the orientation of 45° and exposure time of 100 ms). It can be observed that all reconstruction algorithms effectively reconstruct the part geometry, with Phoenix producing a notably smoother surface compared to other algorithms. In the gray value histograms shown in Fig. 4, two peaks that correspond to air and solid are obvious. In the region between the air and solid peaks of OS-SART and Phoenix, the counts show relatively constant changes. However, an additional peak is observed in the FDK histogram, resulting in significant fluctuations in the counts. Modifying the display in the software, we found that this peak represents the voxels around surfaces (Fig. 5a). Besides, only half of the air peak is observed in the OS-SART histogram, which is attributed to the nonnegative constraints during iterations [21].

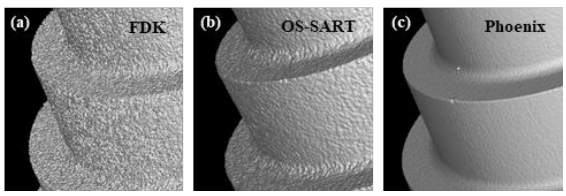

Fig. 3. Voxel models after reconstruction.

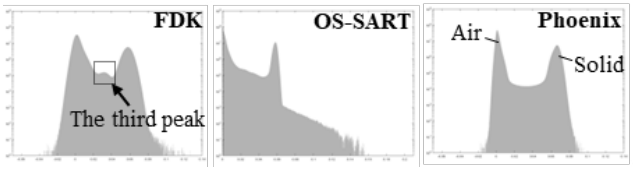

Fig. 4. Histograms of the gray value from three methods.

Since the distribution of the gray values around surfaces is crucial to surface determination, which in turn affects the accuracy of the dimensional measurement, the transition of the gray value across a surface was detected in a cross section, as shown in Fig. 5. The gray values from air to solid are presented in Fig. 6. In voxel modes from Phoenix and OS-SART, the change of gray value is monotonous. However, in the FDK voxel model, the gray value shows higher fluctuations, and a great change of derivative was found in the middle, potentially challenging the surface determination.

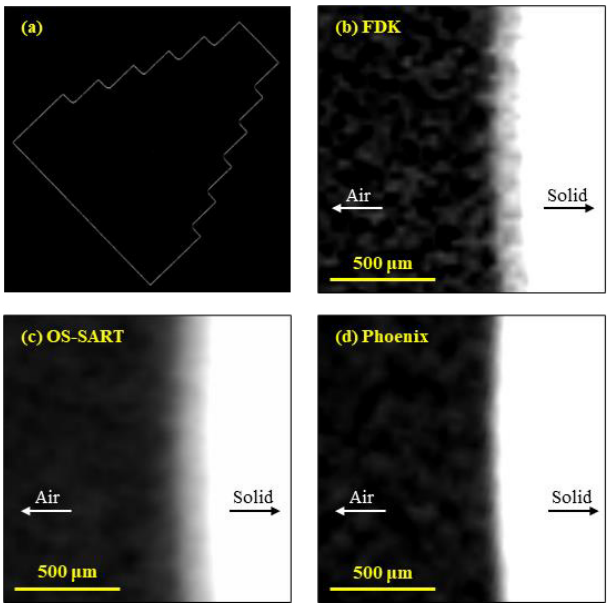

Fig. 5. Change of gray value around the surface.

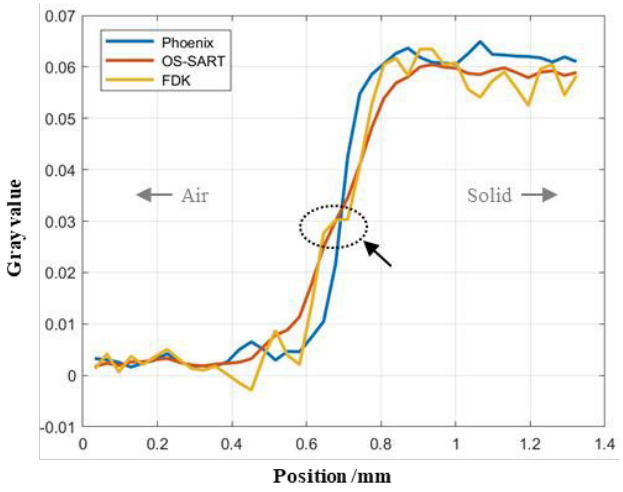

Fig. 6. Gray value transition over a surface.

3.2. Main effects of reconstruction algorithm and parameters

The main effects of the reconstruction algorithm, part orientation, and exposure time on dimensional measurements were analyzed across the features, with the preference for values closer to 0. Through hypothesis testing of one-way ANOVA (α=0.05, H_0: all means are equal; H_1: not all means are equal), significant differences can also be observed. It should be noted that every feature contains 5 or 6 measurands whose nominal values or positions are different.

The impact on diameter is shown in Fig. 7, where the reconstruction algorithm notably influences diameter results. Although Phoenix yields smoother surfaces, it gives worse results of diameters. Significant influence is observed in part orientation, while exposure time exhibits no impact. Additionally, measurands also show influences, probably resulting from the differences in nominal values and position with respect to the optical axis.

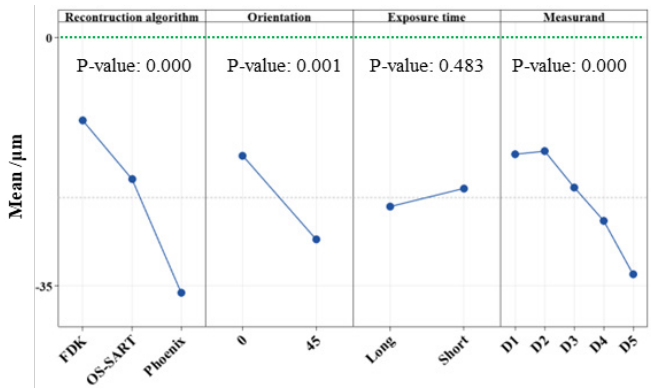

Fig. 7. Main effects plot for diameter error.

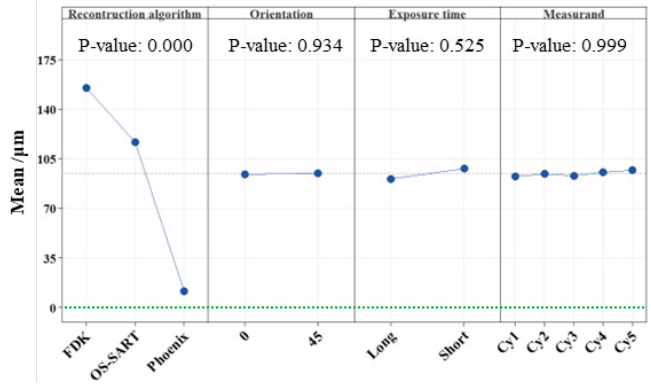

Fig. 8. Main effects plot for cylindricity error.

Fig. 8 shows the impact on cylindricity error, indicating a significant effect of the reconstruction algorithm. This is visually evidenced by the different amount of noise on surfaces generated by the three algorithms (Fig. 3). Besides, orientation, exposure time, and measurand exhibit little influence. In Fig. 9, reconstruction algorithm still plays an important role in flatness measurement. Phoenix gives the best result while FDK yields the worst. Part orientation also affects the flatness, and scans with tilted angle of 45° show less error. This may be coherent with the stronger FDK effect generated by a projection in which the surface is far away from the optical axis [22]. Differences in exposure time and measurands have little impact on the flatness error evaluation.

The hypothesis test of one-way ANOVA was conducted focusing on FDK and OS-SART (α=0.05, H_0: two means are equal; H_1: two means are not equal), with results shown in Table 3. It reveals that while FDK and OS-SART do not exhibit significant differences in diameter measurements, they do show notable distinctions in cylindricity and flatness

measurements. The better performance of OS-SART may be attributed to the iterative updates and compromises of the voxel model with respect to real projection images, resulting in a gray value distribution closer to reality.

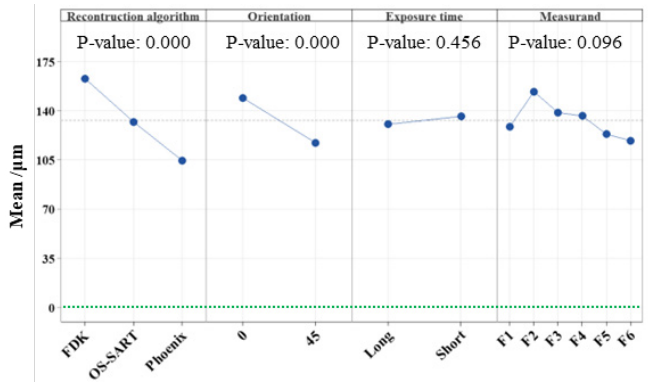

Fig. 9. Main effects plot for flatness error.

Table 3 Hypothesis test on FDK and OS-SART

Features	p-value	Significant difference
Diameter	0.059	No
Cylindricity	<0.001	Yes
Flatness	<0.001	Yes

3.3. Interaction between reconstruction algorithm and parameters

Fig. 10 shows the specific effects of orientation, exposure time, and measurand, with respect to diameter, cylindricity, and flatness error. The hypothesis test of one-way ANOVA was also conducted, and p-values corresponding to the curves from single reconstruction algorithms are presented in the plots.

Regarding diameter, the FDK algorithm is only sensitive to part orientation, showing lower error at 0° compared to 45°. The OS-SART algorithm is unaffected by orientation, exposure time, or measurand. The Phoenix algorithm is relevant to measurand, with a significant error increase from D1 to D5, likely due to nominal value or positional differences.

For cylindricity, all algorithms are insensitive to orientation and measurand. However, FDK and Phoenix show a response to exposure time, with lower error at longer exposures, while OS-SART remains unaffected by exposure time.

Concerning flatness, all algorithms are sensitive to part orientation. All three algorithms exhibit lower error at 45° compared to 0°, while none of them is responsive to exposure time or measurand, possibly due to high voltage in data acquisition ensuring overall image quality. The specific absolute differences of the mean error for each curve are listed in Table 4.

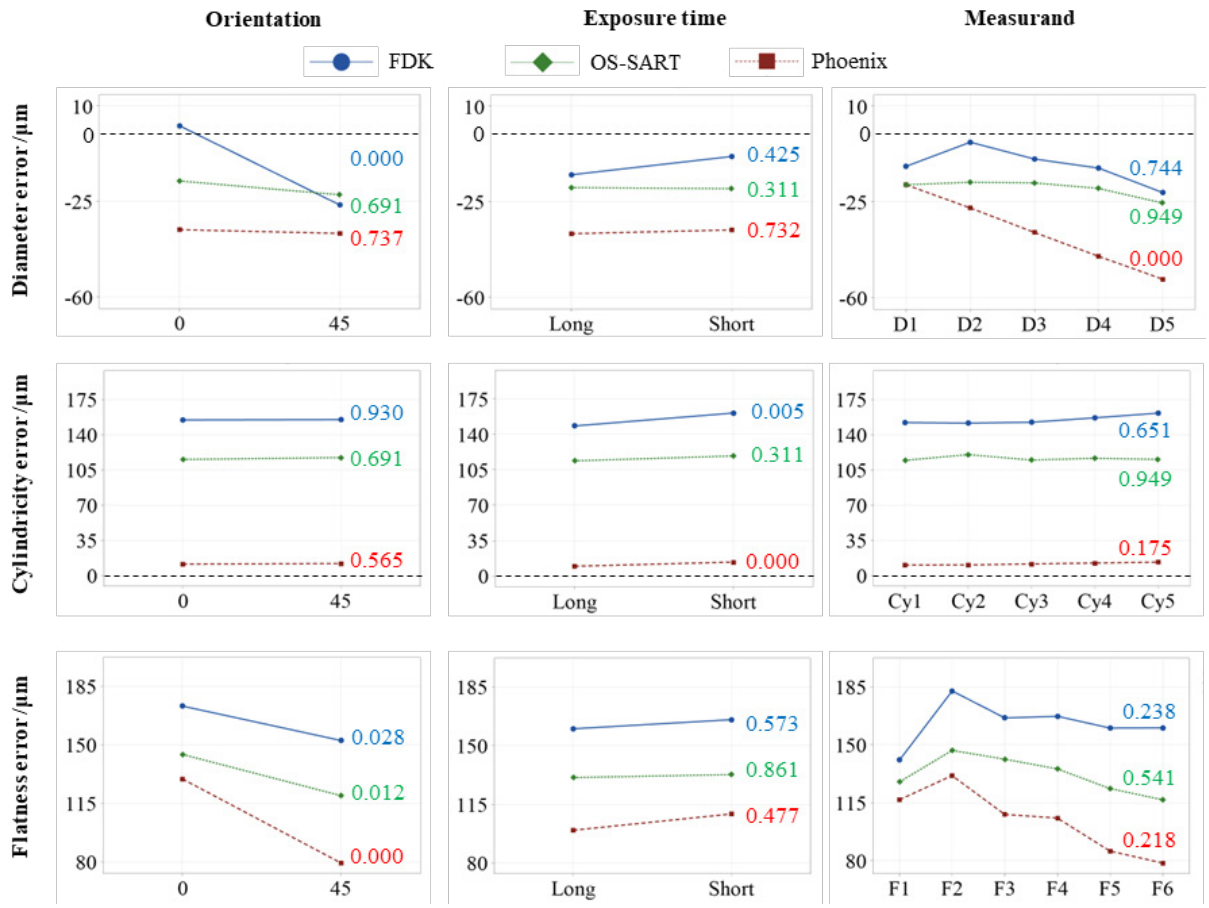

Fig. 10. Specific effect plots of acquisition parameters, with reconstruction algorithms separated. The numbers in the plot are the p-values correspond to curves.

Table 4. The absolute differences of mean values for each curve in Figure. 10. Each element represents the difference for FDK, OS-SART, and Phoenix, respectively. "-" indicates no significant difference.

Features	Difference in orientation /μm	Difference in exposure time /μm	Difference in measurand /μm
Diameter	29 / - / -	- / - / -	- / - / 34
Cylindricity	- / - / -	13 / - / 4	- / - / -
Flatness	21 / 25 / 50	- / - /-	- / - /-

4. Discussion and conclusion

We can further make some inferences regarding selecting reconstruction algorithms and acquisition parameters for XCT geometric measurements. Compared with the results of FDK, OS-SART yields comparable results for diameter, and significantly better results for cylindricity and flatness (Table 3), making it a suitable reconstruction algorithm in this study. As for parameters, the part orientation provides similar effects on all algorithms in cylindricity and flatness results, while yields difference in diameter results, with significant impact on FDK algorithm (Fig. 10). Exposure time always shows similar effects on algorithms in diameter and flatness results. In cylindricity, it has significant influence on FDK but little on OS-SART. It should be noted that since we only considered aluminum as part material in this work, the material influence was not discussed. More materials should be considered in the future to get more robust conclusions.

In conclusion, this work explained the questions we pointed out in the first section to a certain extent. Firstly, algebraic reconstruction algorithms, represented by OS-SART, could be competitive reconstruction algorithms in XCT geometric measurements, despite longer computation time. Secondly, the influence of acquisition parameters on geometric measurements is different between FDK and OS-SART. Studies with more parameters and levels should be performed in the future.

Acknowledgements

We gratefully acknowledge MICS (Made in Italy – Circular and Sustainable) Extended Partnership and received funding from the European Union Next-GenerationEU (Piano Nazionale di Ripresa e Resilienza (PNRR) – Missione 4 Componente 2, Investimento 1.3 – D.D. 1551.11-10-2022, PE00000004). We also express great appreciation for the support of the China Scholarship Council.

References

[1] Yang, F., Zhang, D., Huang, K., et al., 2023. Iterative excitation with noise rejection techniques for X-ray computed tomography of hollow turbine blades. Nondestructive Testing and Evaluation 38.1, 172–188.

[2] Withers, P. J., Bouman, C., Carmignato, S., et al., 2021. X-ray computed tomography. Nature Reviews Methods Primers 1.1, 18.

[3] Dewulf, W., Bosse, H., Carmignato, S., et al., 2022. Advances in the metrological traceability and performance of X-ray computed tomography. CIRP Annals 71.2, 693–716.

[4] Villarraga-Gómez, H., Herazo, E. L., Smith, S. T., 2019. X-ray computed tomography: from medical imaging to dimensional metrology. Precision Engineering 60, 544–569.

[5] Mileto, A., Guimaraes, L. S., McCollough, C. H., et al., 2019. State of the Art in Abdominal CT: The Limits of Iterative Reconstruction Algorithms. Radiology 293.3, 491–503.

[6] Niu, T., Al-Basheer, A., Zhu, L., 2012. Quantitative cone-beam CT imaging in radiation therapy using planning CT as a prior: First patient studies. Medical Physics 39.4, 1991–2000.

[7] Pourmorteza, A., Dang, H., Siewerdsen, J. H., et al., 2016. Reconstruction of difference in sequential CT studies using penalized likelihood estimation. Physics in Medicine & Biology 61.5, 1986.

[8] Ravishankar, S., Ye, J. C., Fessler, J. A., 2020. Image Reconstruction: From Sparsity to Data-Adaptive Methods and Machine Learning. Proceedings of the IEEE 108.1, 86–109.

[9] Jones, G. A., Huthwaite, P., 2018. Limited view X-ray tomography for dimensional measurements. NDT & E International 93, 98–109.

[10] Sun, W., Chretien, S., Biguri, A., et al., 2023. The realisation of fast X-ray computed tomography using a limited number of projection images for dimensional metrology. NDT & E International 137, 102852.

[11] Bussy, V., Vienne, C., Kaftandjian, V., 2023. Fast algorithms based on Empirical Interpolation Methods for selecting best projections in Sparse-View X-ray Computed Tomography using a priori information. NDT and E International 134, 102768.

[12] Villarraga-Gómez, H., Smith, S. T., 2020. Effect of the number of projections on dimensional measurements with X-ray computed tomography. Precision Engineering 66, 445–456.

[13] Villarraga-Gómez, H., Amirkhanov, A., Heinzl, C., et al., 2021. Assessing the effect of sample orientation on dimensional X-ray computed tomography through experimental and simulated data. Measurement 178, 109343.

[14] Villarraga-Gómez, H., Smith, S. T., 2022. Effect of geometric magnification on dimensional measurements with a metrology-grade X-ray computed tomography system. Precision Engineering 73, 488–503.

[15] Rossides, C., Towsyfyan, H., Biguri, A., et al., 2022. Effects of fast x-ray cone-beam tomographic measurement on dimensional metrology. Metrologia 59.4, 044003.

[16] Jerri, A. J., 1977. The Shannon sampling theorem—Its various extensions and applications: A tutorial review. Proceedings of the IEEE 65.11, 1565–1596.

[17] Feldkamp, L. A., Davis, L. C., Kress, J. W., 1984. Practical cone-beam algorithm. JOSA A 1.6, 612–619.

[18] Wang, G., Jiang, M., 2004. Ordered-subset simultaneous algebraic reconstruction techniques (OS-SART). Journal of X-Ray Science and Technology 12.3, 169–177.

[19] Biguri, A., Dosanjh, M., Hancock, S., et al., 2016. TIGRE: a MATLAB-GPU toolbox for CBCT image reconstruction. Biomedical Physics & Engineering Express 2.5, 055010.

[20] Borges de Oliveira, F., Stolfi, A., Bartscher, M., et al., 2016. Experimental investigation of surface determination process on multi-material components for dimensional computed tomography. Case Studies in Nondestructive Testing and Evaluation 6, 93–103.

[21] Byrne, C., 2005. Choosing parameters in block-iterative or ordered subset reconstruction algorithms. IEEE Transactions on Image Processing 14.3, 321–327.

[22] Xue, L., Suzuki, H., Ohtake, Y., et al., 2015. Numerical Analysis of the Feldkamp–Davis–Kress Effect on Industrial X-Ray Computed Tomography for Dimensional Metrology. Journal of Computing and Information Science in Engineering 15.2, 021008.